Free-space optical data links based on coaxial sidelobe-modified optical vortices

Meng Zhang (张 萌)[1], Ping Jia (贾 平)[1], Yuru Li (李玉茹)[2], Ting Lei (雷 霆)[3], Zhaohui Li (李朝晖)[2], and Xiaocong Yuan (袁小聪)[3,*]

[1]*Institute of Modern Optics, Nankai University, Tianjin 300071, China*
[2]*Institute of Photonics Technology, Jinan University, Guangzhou 510632, China*
[3]*Institute of Micro & Nano Optics, Key Laboratory of Optoelectronic Devices and Systems of Ministry of Education and Guangdong Province, College of Optoelectronic Engineering, Shenzhen University, Shenzhen 518060, China.*
**Corresponding author: xcyuan@szu.edu.cn*

Received June 26, 2015; accepted August 19, 2015; posted online September 17, 2015

We propose and demonstrate free-space optical data links based on coaxial sidelobe-modified optical vortices (CSMOVs). In contrast to the optical communication systems based on amplitude, frequency, or phase detection, the proposed scheme uses the radii ratio between the principle ring and the first sidelobe of the CSMOV. Therefore, the demand of stringent alignment and/or accurate phase matching is released. We design and optimize a composite computer-generated hologram to generate a CSMOV with four topological charges (TCs). Extracted from the images captured by a CCD camera, the radii ratio between the principle ring and the first sidelobe of different TCs are consistent with the theoretical values.

OCIS codes: 050.4865, 060.4510, 090.2890.
doi: 10.3788/COL201513.100502.

Since Allen first proposed that beams with a phase term of $\exp(i\ell\theta)$ have an orbital angular momentum (OAM) of $\ell\hbar$ per photon in 1992[1] [ℓ refers to the topological charge (TC) and θ is the azimuthal angle in polar coordinates], optical vortices (OVs) have widely been applied in optical trapping[2–4], generation of cylindrical vector beams[5–8], and optical communications[9–17]. Due to its infinite set of orthogonal states and high security derived from the uncertainty relationship between angular position and TC[18], OAM has been demonstrated as a new degree of freedom in optical data transmission systems. OAM is used either as division multiplexing (OAM-DM) to increase the capacity of a communication system[19,20] or as encoding to enhance security in data transmission[9,10,21]. In 2012, Wang *et al.*[19] employed four OVs with different TCs in free-space optical (FSO) communication systems to achieve a high information transmission capacity of 1.37 Tbit/s and a spectral efficiency of 25.6 bit/s/Hz. In their experiment, the four states of OAM were demultiplexed by a spatial light modulator (SLM) with a conjugate phase mask. In 2013, terabit-scale data transmissions were achieved over 1.1 km based on OAM-DM in specialty fiber[20]. The demultiplexing system coupled OV beams into free space again and sorted the OAM states according to their TCs by a SLM. Recently, our group demonstrated parallel detection of ten multiplexed OAM channels for FSO communication using Dammann optical vortex gratings[15]. In the aforementioned OV communication systems based on interference or phase-matching detection, stringent alignment in the receiving system is required, which strongly reduces the flexibility of communication systems[9–14,19,20,22,23]. To solve this problem, in our previous work[21] we reported a method for FSO data links where the transmitter encoded data into a composite computer-generated hologram (CCGH) and the receiver decoded data by retrieving an array of sidelobe-modulated OV (SMOV). The measurement of OAM in this method only depends on robustness of the radii ratio in SMOV transmission, thus releasing the high demand of alignment and making the detecting system simpler and more stable. However, this method diffracts the OV beam into a 2D array, so the required detection area of the SMOV array magnifies with increasing propagation distance. Furthermore, the arrayed rings complicated the demodulation system compared to the coaxial beam solution.

In this Letter, we present a new approach for the FSO data links employing a coaxial SMOV (CSMOV) beam that are generated by CCGH. After propagating in free space, the carried information is demultiplexed by extracting the radii ratios of the principle rings and the overlapping first sidelobe rings in the CSMOV. The robustness of the radii ratio in CSMOV transmission guarantees the receiver unit against the difficulties and instabilities caused by the stringent alignment and accurate phase matching. Improved from the SMOV array, this method offers even lower demand than that in Ref. [21] for demodulation systems. It is noted that such a coaxial beam could provide a high spatial efficiency and make it promising to propagate in a specially-designed fiber in the future.

We use the SLM to create the CSMOV beams comprising OVs with different TCs. All of these OVs have commonly located sidelobes and separate principle rings serving as communication channels in the system. By switching the CCGH, the modulated signals can be individually uploaded to each channel of the CSMOVs. At the

downstream, the signals from coaxial OV beams are detected by a CCD. The images obtained by the CCD are uploaded onto another computer to read out the transmitted signals by calculating the radii ratio of the principle and the first sidelobe rings in the CSMOV.

Figure 1 depicts the experimental system. The signal generation unit consists of a laser (532 nm) and a computer-controlled reflective phase type SLM (Holoeye LC-R3000, 1920 pixels × 1200 pixels). The light beam incidents on to the SLM after collimation and expansion. The Gaussian beam is converted into a CSMOV beam by the SLM loaded with a CCGH. By modulating the CCGH on the SLM continuously, data can be uploaded onto different channels in the CSMOV beam. We use a CCD camera (3.2 μm × 3.2 μm per pixel, 2048 pixels × 1536 pixels) to capture the CSMOV patterns and demultiplex the signal with PC2.

Figure 2 shows the simulation results of the CSMOV with four TCs. Figure 2(a) illustrates a coaxial OV beam combining four SMOVs with small TC intervals ($\ell = 41$, 43, 47, and 49). The radii of the principle rings are proportional to $\sqrt{\ell}$[9] [as the four rings shown in the corners of Fig. 2(a)]. The sidelobes and/or the principle ring interfere with each other, which produces an interference pattern [as shown in the central pattern of Fig. 2(a)] and makes the detection of the radius ratio difficult. In addition, the intensity of the sidelobe is much weaker than the principle ring, which also increases the difficulty for extracting the radii of sidelobes. In order to solve these problems, we choose SMOVs with large enough TCs intervals ($\ell = 30$, 60, 80, and 100) and push their sidelobes to a common overlapped position while keeping the principle ring position unchanged. Based on these improvements, we can push and superimpose the sidelobes at the same ring to re-encode the radii ratio between the principle rings and the first sidelobe rings of the CSMOV. Therefore, SMOV beams with different TCs identified by the different radii ratio in the CSMOV are able to carry multiple channels of data in transmission. In the detecting terminal, in principle we can realize a high-speed real-time detection by using a linear photodiode (PD) array, which greatly simplifies the detection system. In this experiment,

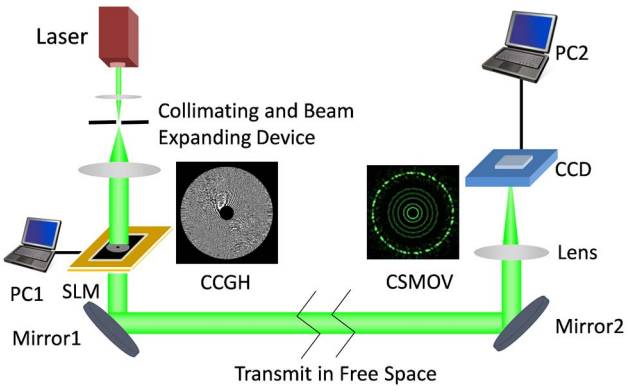

Fig. 1. Experimental setup of CSMOV-based optical data links.

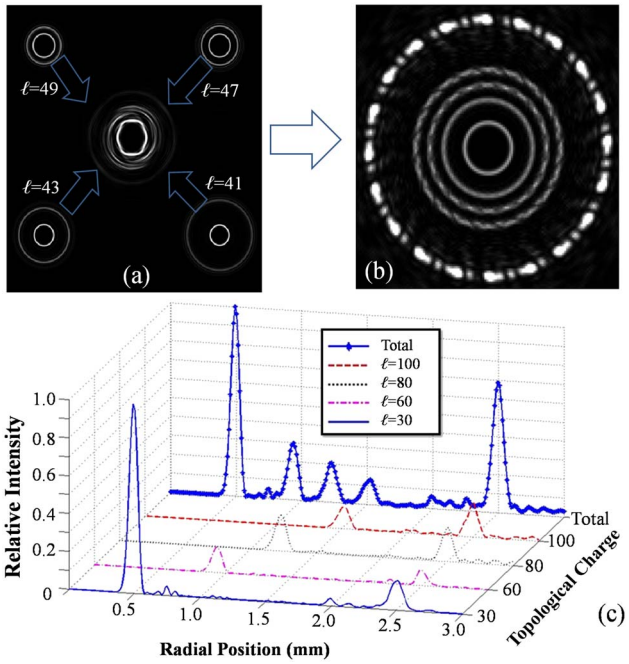

Fig. 2. Simulated intensity distribution of the SMOVs (a) with $\ell = 41, 43, 47, 49$ and (b) with $\ell = 30, 60, 80, 100$. (c) Theoretical intensity distribution of the SMOVs with $\ell = 30$, 60, 80, 100. The peaks around $\rho_1 = 2.50$ mm refer to the sidelobe rings, the other 4 peaks ($\rho_i = 0.50$, 0.95, 1.23, 1.53 mm) from left to right refer to the principle rings of the TC from 30 to 100, and the radii ratio is 0.20, 0.38, 0.49, 0.61, respectively. The curve labeled as "Total" in (c) shows the intensity distribution when four states of SMOV are used to form a CSMOV. Since each SMOV owns relatively equal total energy while the circumference of its principle ring increases with TC, the principle ring of the larger TC obtains a lower intensity.

we use a CCD to prove the concept of this system. In the receiver unit of our FSO data links there is no need for extra complex decoding devices, such as sophisticated holograms or multi-pinholes, which greatly overcome the drawbacks caused by strict alignment and phase matching between the OVs beams and optical elements.

Following our previous work[12,24], we divide the circular spiral phase plate into several annular areas in accordance with the ratio $\beta = \rho_1/\rho_i$, where ρ_1 and ρ_i stand for the principle and the first sidelobe ring's radii of the Fraunhofer diffraction intensity distribution of the circular spiral phase plate, respectively. Each annular area is a ring-shaped spiral phase plate. Here, we only use the outermost $N+1$ annular spiral phase plate, and N is a positive integer, while other regions are equivalent to nontransparent. In our experiment, we found the best result with $N = 5$. We superimpose different radial phase modulations in each annular spiral phase plate in order to encode the radii ratio between the principle ring and modulated sidelobe of the Fraunhofer diffraction intensity distribution. Therefore, this compound spiral phase structure of the complex transmittance function can be expressed as

Table 1. Design Parameters of CSMOV for Each Annular Aperture

ℓ	ρ_1/ρ_i	α_1	α_2	α_3	α_4	α_5	Theoretical Value of the Radii Ratios ρ_1/ρ_2	Experimental Value of the Radii Ratios	Error (%)
30	0.7874	53.5	49.3	53.3	59.6	41.6	0.200	0.1947	2.65
60	0.8552	48.8	59.7	52.1	45.4	37.6	0.378	0.38	0.52
80	0.8780	57.5	39.9	42.8	36.4	21.6	0.495	0.4952	0.04
100	0.8936	39.7	34.4	22.5	15.5	16.2	0.611	0.6112	0.03

$$\varphi_i = \sum_{m=0}^{N}\left[\mathrm{circl}\left(\frac{r}{\beta^m R}\right) - \mathrm{circl}\left(\frac{r}{\beta^{m+1} R}\right)\right] \times e^{i\ell\theta + i\alpha_m \omega r},$$
$$\mathrm{circl}(x) = \begin{cases} 1 & \text{if } x < 1 \\ 0 & \text{if } x \geq 1 \end{cases}, \tag{1}$$

where φ_1 is the phase distribution of the CCGH of the SMOV, ℓ is a TC of the spiral phase structure, (r, θ) are the polar coordinates on the plane of the phase device, R is the outer radius of the spiral phase structure, $\omega = \pi/R$, β is the radius ratio between the inner and outer annular helical phase structure ($\beta = \rho_1/\rho_i$), circl(x) is defined as the function of a circle with radius x, and a_m is the radial phase modulation parameter in the mth annular spiral phase plates that pushes different sidelobes to the desired position (the radius of sidelobe is ρ_2). It is noted that $a_0 \equiv 0$, which means that the outermost annular spiral phase structure is not modulated with the radial parameter and the principle rings do not move. We obtain the optimized a_1 to a_m by using the trial-and-error method, according to Ref. [20]. Table 1 shows the design parameters of the SMOV for each annular aperture. We obtain SMOVs with four TCs with different radii ratio between the principle ring and the sidelobe (ρ_1/ρ_2). Figure 2(c) shows the theoretical SMOV intensity distribution using the design parameters listed in Table 1. The results verify the feasibility of our method. Sidelobes of different TCs move to the same position ($\rho_2 = 2.5$ mm), while the principle rings are kept apart.

In our experiment, we use a phase-only hologram to produce a CSMOV with TCs of 30, 60, 80, and 100. The complex amplitude of the CSMOV can be expressed as

$$\Psi = \sum_{n=1}^{N} E_{\ell_n} \varphi_{\ell_n}, \tag{2}$$

where $N = 4$, ℓ_1 to ℓ_4 equals 30, 60, 80, and 100, respectively, φ_{ℓ_n} is the CCGH of the SMOV with TC $= \ell_n$, E_{ℓ_n} is the normalized amplitude weight of each SMOV, and $\Sigma_{n=\ell}^{N} |E_{\ell_n}|^2 = 1$. With the increase of TC, the principle ring reduces its intensity [as shown in Fig. 2(c)] due to the larger circumference of the ring. In order to get enough intensity, the E_{ℓ_n} with a greater TC should have a larger weight. In our experiment, we choose that

$$|E_{30}|:|E_{60}|:|E_{80}|:|E_{100}| = 0.077:0.308:0.546:0.775, \tag{3}$$

to get an almost equal intensity of the principle rings. Since we use a phase-only SLM in our experiment, we must obtain a phase-only expression to generate a CSMOV. We assume that

$$\varphi = \mathrm{angle}\left(\sum_{n=\ell}^{N} B_{\ell_n} \varphi_{\ell_n}\right), \tag{4}$$

$$\Psi = \exp(i\varphi) = \sum_{n=\ell}^{N} A_{\ell_n} \varphi_{\ell_n}. \tag{5}$$

By optimizing the B_{ℓ_n}, we make the ratio of A_{ℓ_n} close to the ratio of E_{ℓ_n}.

We use a CSMOV with different TCs as channels to carry data. By measuring the radius ratio, we decode information in different channels. Figure 3 shows the experimental scheme and results of CSMOV-based data links. Figures 3(a1)–3(e1) depict the intensity distributions of the generated CSMOV captured by the CCD experimentally. In order to decode data information randomly generated by PC1 in Fig. 1, we need to extract the radii ratios from the captured images. However, due to the interference, CSMOV shows an alternative bright and dark spot pattern along the sidelobe ring. We filter out the noise,

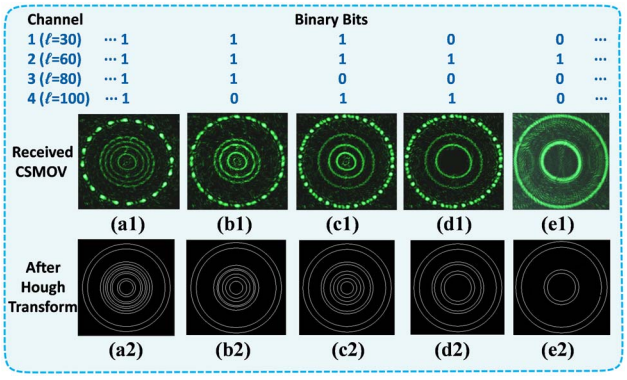

Fig. 3. Bits in channels and their corresponding CCGH, CSMOV, and identified rings. For a given channel, the on/off of the SMOV with the corresponding TC represents 1/0 of information. (a1)–(e1) are the experimental results of CSMOVs carrying information on the top and (a2)–(e2) are the results after Hough transform.

rotate the images obtained by the CCD clockwise, and superimpose the rotated images with different angles. As a result, we eliminate the inhomogeneous outermost ring due to the interference between the sidelobes and the asymmetry of the inner principle rings induced by the imaging lens. Finally, we can get relatively ideal concentric rings through binarization. We use a Hough transform[25] to identify the radii of rings, which are used to calculate radii ratios and decode information in different channels. Figures 3(a2)–3(e2) show the boundary of the rings identified by the Hough transform algorithm.

Table 1 also shows the results in comparison with the theoretical values by the radii ratios identified through the Hough transform and the errors in percentage. We attribute the errors to the distortion of the images and the Hough transform algorithm. For a given channel, on/off of the SMOV corresponds to 1/0 of the bitstream. After a transmission coaxially in free space, the CSMOV are captured by a CCD camera. What we received are different combinations of the four SMOVs [as shown in Fig. 3(a1)–3(e1)]. Then the radii ratios of each SMOV are extracted to determine the TC of the channels and the transmitted data is decoded. In the data link experiment, a pseudorandom code stream of 5000-bit length is transmitted for multiple times without error bits detected. We estimate that the OAM communication system has a bit error rate (BER) of less than 2.0×10^{-4}. In the current condition, the error bit can be corrected by the typical forward error correction algorithm. The BER mainly comes from atmospheric turbulence and background noise in free space. In our previous work, we theoretically analyzed the influence of weak, medium, and strong turbulence for OAM communication in the atmosphere[15]. In weak and medium atmospheric turbulence, the OAM signals can propagate for 1 km with acceptable cross talk. Here, in the proof of concept demonstration, the OAM signal channels are only several meters long. Therefore, the turbulence of the atmosphere is very weak and can be ignored. Background noise can reduce the contrast of the image, which may cause errors in radii identification. We also calculate the cross talk of the system. The cross talk between the CSMOV channels can be expressed as

$$\text{Crosstalk(dB)} = 10\ \lg\left(\frac{P_{XT}}{P_{\ell_i}}\right), \tag{6}$$

where P_{XT} is the intensity received at the radial position of the channel when only the desired channel is off and P_{ℓ_i} is the intensity received at the same position when only the desired channel is on.

There is an example shown in Fig. 4(a) for a TC of 80 and a radial position of 1.24 mm. The theoretical and experimental results are shown in Fig. 4(b). The black bars represent the theoretical results while the red bars represent experimental results. The experimental data agrees with the theoretical values. The maximum cross talk is less than −15 dB, which means that P_{XT} is less than $0.03 \times P\ell_i$. After the subsequent image processing, the cross talk almost makes no contribution to the BER.

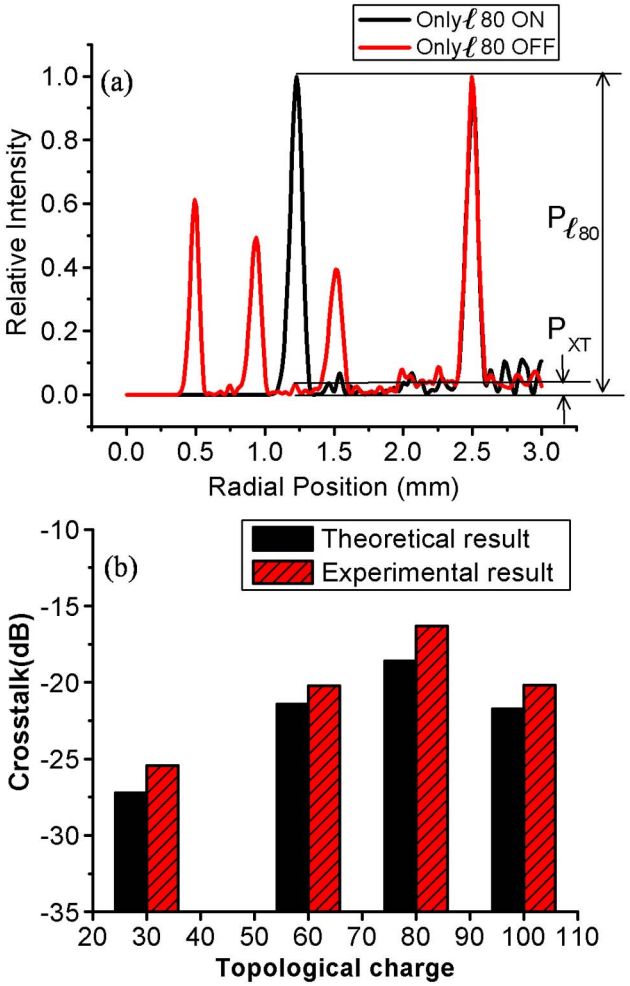

Fig. 4. (a) Relative intensity distribution when the CSMOV channel with TC = 80 is on/off; here, the measured radial position is 1.24 mm. (b) The theoretical and experimental results of cross talk of four CSMOV channels with TC = 30, 60, 80, 100, respectively.

In conclusion, we propose and demonstrate a new method of FSO data links based on CSMOV. We use improved CCGH to generate CSMOV with different TCs as multiple information channels. At the receiver end, we decode information by calculating radii ratios between the principle and the first sidelobe rings of the CSMOV to avoid strict alignment and phase-matching requirements. In our proof-of-concept experiment, we realize a data transmission in four channels with a BER as low as 2.0×10^{-4} in the proposed system. Potentially, in free space, such a coaxial beam provides the possibility for transmission in specially-designed optical fibers that might have wider applications in modern communication. The demonstrated transmission rate in our experiment is limited by the refreshing rate of the SLM and the CCD. We can use phase plates with high-speed independent controllable light sources and a linear PD array to realize high-speed signal encoding and detection.

This work was partially supported by the National Nature Science Foundation of China (Nos. 61138003, 61427819, and 61405121), the Natural Science Foundation of SZU (No. 201454), and the startup funding of SZU (Nos. 000011, 000075).

References

1. L. Allen, M. W. Beijersbergen, R. J. C. Spreeuw, and J. P. Woerdman, Phys. Rev. A **45**, 8185 (1992).
2. H. He, M. E. J. Friese, N. R. Heckenberg, and H. Rubinszteindunlop, Phys. Rev. Lett. **75**, 826 (1995).
3. J. E. Curtis, B. A. Koss, and D. G. Grier, Opt. Commun. **207**, 169 (2002).
4. K. Ladavac and D. G. Grier, Opt. Express **12**, 1144 (2004).
5. Q. W. Zhan, Adv. Opt. Photonics **1**, 1 (2009).
6. Q. W. Zhan, Opt. Lett. **31**, 867 (2006).
7. L. Allen, J. Courtial, and M. J. Padgett, Phys. Rev. E **60**, 7497 (1999).
8. Z. Fang, Y. Yao, K. Xia, and J. Li, Chin. Opt. Lett. **13**, 031405 (2015).
9. G. Gibson, J. Courtial, M. J. Padgett, M. Vasnetsov, V. Pas'ko, S. M. Barnett, and S. Franke-Arnold, Opt. Express **12**, 5448 (2004).
10. G. Gibson, J. Courtial, M. Vasnetsov, S. Barnett, S. Franke-Arnold, and M. Padgett, Proc. SPIE **5550**, 367 (2004).
11. Z. Bouchal and R. Celechovsky, New J. Phys. **6**, 131 (2004).
12. J. Lin, X. C. Yuan, S. H. Tao, and R. E. Burge, Appl. Opt. **46**, 4680 (2007).
13. Y. D. Liu, C. Q. Gao, M. W. Gao, X. Q. Qi, and H. Weber, Opt. Commun. **281**, 3636 (2008).
14. C. S. Guo, S. J. Yue, and G. X. Wei, Appl. Phys. Lett. **94**, 231104 (2009).
15. T. Lei, M. Zhang, Y. R. Li, P. Jia, G. N. Liu, X. G. Xu, Z. H. Li, C. J. Min, J. Lin, C. Y. Yu, H. B. Niu, and X. C. Yuan, Light Sci. Appl. **4**, e257 (2015).
16. Y. Zhu and F. Zhang, Chin. Opt. Lett. **13**, 030501 (2015).
17. Y. Li, H. Yang, J. Liu, L. Gong, Y. Sheng, W. Cheng, and S. Zhao, Chin. Opt. Lett. **11**, 021104 (2013).
18. S. Franke-Arnold, S. M. Barnett, E. Yao, J. Leach, J. Courtial, and M. Padgett, New J. Phys. **6**, 103 (2004).
19. J. Wang, J. Y. Yang, I. M. Fazal, N. Ahmed, Y. Yan, H. Huang, Y. X. Ren, Y. Yue, S. Dolinar, M. Tur, and A. E. Willner, Nat. Photonics **6**, 488 (2012).
20. N. Bozinovic, Y. Yue, Y. X. Ren, M. Tur, P. Kristensen, H. Huang, A. E. Willner, and S. Ramachandran, Science **340**, 1545 (2013).
21. P. Jia, Y. Yang, C. J. Min, H. Fang, and X. C. Yuan, Opt. Lett. **38**, 588 (2013).
22. J. Leach, M. J. Padgett, S. M. Barnett, S. Franke-Arnold, and J. Courtial, Phys. Rev. Lett. **88**, 257901 (2002).
23. J. Leach, J. Courtial, K. Skeldon, S. M. Barnett, S. Franke-Arnold, and M. J. Padgett, Phys. Rev. Lett. **92**, 013601 (2004).
24. J. Chen, X. Zhao, Z. L. Fang, S. W. Zhu, and X. C. Yuan, Opt. Lett. **35**, 1485 (2010).
25. P. V. C. Hough, "Method and Means for Recognizing Complex Patterns," U.S. Patent 3069654 (1962).